British Geological Survey
NATURAL ENVIRONMENT RESEARCH COUNCIL

Characteristics of geoeffective CMEs - guidelines for Space Weather forecasting

Earth Hazards and Observatories Programme
Internal Report IR/18/021

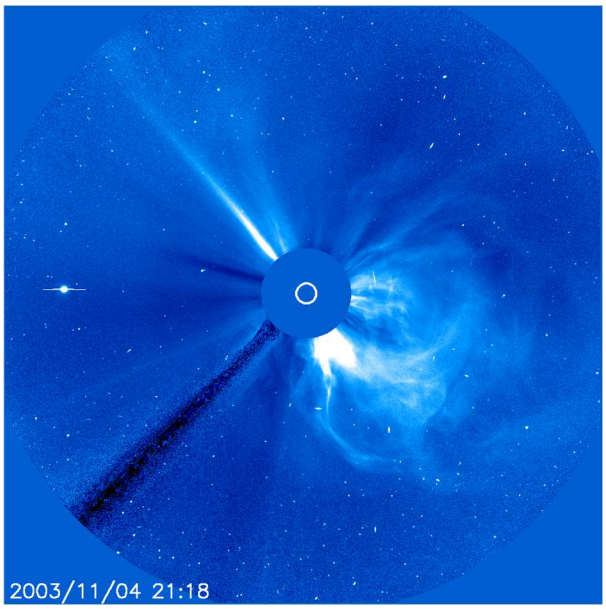

BRITISH GEOLOGICAL SURVEY

EARTH HAZARDS AND OBSERVATORIES PROGRAMME

INTERNAL REPORT IR/18/021

Characteristics of geoeffective CMEs - guidelines for Space Weather forecasting

G S Richardson

Keywords

Space Weather, Forecasting, Coronal Mass Ejections.

Front cover

An example of a LASCO image showing a CME, credit: ESA/NASA SOHO/LASCO.

Bibliographical reference

G S RICHARDSON. 2018. Characteristics of geoeffective CMEs - guidelines for Space Weather forecasting. *British Geological Survey Internal Report*, IR/18/021. 28pp.

Keyworth, Nottingham British Geological Survey 2019

BRITISH GEOLOGICAL SURVEY

The full range of our publications is available from BGS shops at Nottingham, Edinburgh, London and Cardiff (Welsh publications only) see contact details below or shop online at www.geologyshop.com

The London Information Office also maintains a reference collection of BGS publications, including maps, for consultation.

We publish an annual catalogue of our maps and other publications; this catalogue is available online or from any of the BGS shops.

The British Geological Survey carries out the geological survey of Great Britain and Northern Ireland (the latter as an agency service for the government of Northern Ireland), and of the surrounding continental shelf, as well as basic research projects. It also undertakes programmes of technical aid in geology in developing countries.

The British Geological Survey is a component body of the Natural Environment Research Council.

British Geological Survey offices

BGS Central Enquiries Desk

Tel 0115 936 3143 Fax 0115 936 3276

email enquiries@bgs.ac.uk

Environmental Science Centre, Keyworth, Nottingham NG12 5GG

Tel 0115 936 3241 Fax 0115 936 3488

email sales@bgs.ac.uk

The Lyell Centre, Research Avenue South, Edinburgh EH14 4AP

Tel 0131 667 1000 Fax 0131 668 2683

email scotsales@bgs.ac.uk

Natural History Museum, Cromwell Road, London SW7 5BD

Tel 020 7589 4090 Fax 020 7584 8270

Tel 020 7942 5344/45 email bgslondon@bgs.ac.uk

Columbus House, Greenmeadow Springs, Tongwynlais, Cardiff CF15 7NE

Tel 029 2052 1962 Fax 029 2052 1963

Maclean Building, Crowmarsh Gifford, Wallingford OX10 8BB

Tel 01491 838800 Fax 01491 692345

Geological Survey of Northern Ireland, Department of Enterprise, Trade & Investment, Dundonald House, Upper Newtownards Road, Ballymiscaw, Belfast, BT4 3SB

Tel 028 9038 8462 Fax 028 9038 8461

www.bgs.ac.uk/gsni/

Parent Body

Natural Environment Research Council, Polaris House, North Star Avenue, Swindon SN2 1EU

Tel 01793 411500 Fax 01793 411501

www.nerc.ac.uk

Website www.bgs.ac.uk

Shop online at www.geologyshop.com

Foreword

This report is the published product of a study by the British Geological Survey (BGS) into geomagnetic storm statistics for the purposes of improving our space weather forecasting knowledge.

Acknowledgements

Several individuals have freely given their advice, and provided the local knowledge so important to space weather forecasting. Key staff have helped to review draft chapters of this report. Of the many individuals who have contributed to the project I would particularly like to thank the BGS space weather forecasting team and Dr Alan Thomson.

The author would like to thank the international bodies that make space weather data available, i.e. NASA, ESA and NOAA and the other bodies and organisations that have developed catalogues and tools for space weather analysis, including the CDAW Data Center by NASA, The Catholic University of America, the Naval Research Laboratory, and the University of New Hampshire. This paper also uses data from the CACTus CME catalog, generated and maintained by the SIDC at the Royal Observatory of Belgium.

Contents

FIGURES

TABLES

Summary

Forecasts of geomagnetic activity are important for decision makers tasked with protecting vulnerable technological infrastructure from space weather. However, in the current operational forecast situation there may be relatively little near real-time data with which to make an immediate decision about the level of expected activity. Whilst advances in physical modelling techniques (for example, the WSA-ENLIL model) and increases in the number of different data sources and their availability are improving the situation, there remains a knowledge gap and forecasts still depend heavily on the judgement of the forecaster. The aim of this work is therefore to help space weather forecasters put coronal mass ejection (CME) reports into context, based on an analysis of past events.

I have analysed 12 years of CMEs from Jan 1998 to Dec 2009, with a focus on the data available at the time of CME observation for forecasting. CMEs which, at the time of their observation, were identified as having a potential to impact the Earth have been assessed and correlated with resulting geomagnetic activity, based on the Kp index and NOAA G-scales. 45% of Earth-directed CMEs resulted in geomagnetic storms where Kp reached at least 6- (G2).

Earth-directed CMEs that originated in the western heliohemisphere were more likely to become geoeffective, with 71% of those between heliolongitudes of 15º and 25º resulting in geomagnetic storms; however, CMEs near the limbs were also capable of becoming geoeffective. The percentage of Earth-directed CMEs which became geoeffective increased with increasing velocity, although there is a marked difference between the near real-time velocity estimates (from the real-time CACTus catalog) and the post event “definitive” LASCO catalog velocities. The results presented here will help in determining the likely geoeffectiveness of CMEs in an operational forecast environment.

1 Introduction

Coronal mass ejections (CMEs) are known to be important drivers of space weather, and are responsible for the largest geomagnetic storms (e.g. Brueckner et al., 1998; Gopalswamy, et al., 2007; Zhang, et al., 2007). Large geomagnetic storms can be damaging to ground-based technological infrastructure, so more effective methods of predicting such storms are vitally important.

Accurate prediction of geomagnetic storms is still difficult, at least in part due to the poorly understood nature of CME generation and an inability to identify imminent solar eruption events (Schwenn, et al., 2005). Even when a CME has been observed, it still may not hit the Earth, and if it does the orientation of the interplanetary magnetic field may not be favourable for the generation of a geomagnetic storm. The situation is further complicated by the fact that almost all observed CME properties are subject to projection effects due to the two dimensional nature of coronagraph images (Cremades & St. Cyr, 2007).

Understanding the properties of CMEs shortly after they leave the Sun could provide key information to help predict geomagnetic storms with around 2-3 days warning, and there have been several attempts to do this (e.g. Srivastava & Venkatakrishnan, 2004; Song, et al., 2006; Kim, et al., 2010).

Many studies start with storms or interplanetary coronal mass ejection (ICME) signatures at Earth then work backwards to infer the source parameters (e.g. Zhang et al., 2007; Richardson & Cane, 2010). Others focus only on halo, or partial halo CMEs, where the CME is seen to fully surround the occulting disk (e.g. Wang et al., 2002; Gopalswamy et al., 2007; Kim et al., 2010; Shen et al., 2014). Previous studies suggest fast halo CMEs close to the centre of the disk are favourable candidates for strong storms (Venkatakrishnan & Ravindra, 2003; Kim et al., 2005), and Gopalswamy, et al. (2007) demonstrated that around 71% of frontside halo CMEs were geoeffective. However, some studies have shown that the relationship between CME properties and storm magnitude is unclear. For example, Cane, et al., (2000) reported that only around half of frontside halo CMEs encounter the Earth and only a subset of these result in even moderate geomagnetic activity, whilst Yermolaev & Yermolaev (2006, and references therein) found conflicting estimates of geoeffectiveness of halo CMEs from around 35% to 100%, which may be a result of differing definitions of halo CMEs. Full halo CMEs only make up about 3.6% of all CMEs (Gopalswamy, et al., 2007) and non-halo CMEs are known to be able to become geoeffective. With this in mind the study presented here is not limited to either halo or partial halo CMEs, nor investigation restricted to only those CMEs that caused storms.

The one aspect all the studies mentioned above have in common is that they are based on "definitive" CME parameters. These are characteristics of the CME which are determined after the event, usually through careful, manual evaluation of all imagery and data sources, some of which are not available in near real-time. Whilst these types of studies are vitally important for improving our scientific understanding of the process, in an operational forecast situation a statistical approach based on information available in near real-time is likely to be of more use.

Recent models for predicting CME arrivals, such as the WSA-Enlil model[1], (Arge & Pizzo, 2000; Arge, et al., 2004; Odstrcil, 2003) and the drag-based model (DBM)[2] (Vrnsak & Zic, 2007; Vrnsak, et al., 2012), are useful tools in helping to determine, (a) if a CME is likely to hit the Earth, and (b) an estimate of the time it will arrive. However, in a real-time operational setting the data required to establish the modelling inputs may not be immediately available, and the models themselves can take many hours to run. This can be a problem, particularly for the fastest CMEs.

[1] http://www.swpc.noaa.gov/wsa-enlil/
[2] http://oh.geof.unizg.hr/DBM/dbm.php

Therefore a statistical approach is still of value in an operational context to help a forecaster get a sense of the potential extent of geomagnetic activity resulting from a CME, based on the available real-time data at the time of the forecast.

Here I present statistics on Earth-directed CMEs and their likelihood to cause geomagnetic storms based on near real-time data to recreate an operational forecast situation. For the purposes of this study a geomagnetic storm is defined as having reached a Kp value of 6- (G2) or greater. In Section 1.1 I outline the data sources available, and discuss the process used for selecting Earth-directed CMEs in Section 1.2. In Section 2 I investigate the influence of source location, velocity, and associated flares and filaments on CME geoeffectiveness. These parameters are discussed in context with a number of related studies.

1.1 OPERATIONAL DATA

There are many resources available at present for operational space weather forecasts and for reviewing past events. The following have all been used in this study to help identify past CMEs and geomagnetic events:

1. Images from the Large Angle and Spectrometric Coronograph Experiment (LASCO)[3] instrument on board the Solar and Heliospheric Observatory (SOHO)[4] - LASCO provides coronagraph images of the solar corona from 1.1 to 32 solar radii and allows coronal mass ejections to be observed and studied. Also on board SOHO is the Extreme ultraviolet Imaging Telescope (EIT) which takes direct images of the Sun using filters to examine different layers of the Sun's outer atmosphere.
2. The Computer Aided CME Tracking software (CACTus) (Robbrecht, et al., 2009) is an automated method for detecting CMEs (in near real-time) in the LASCO coronagraphs, and estimating their onset time, duration of lift-off, principle angle (from North) and angular width. The software also determines a velocity in each direction, θ, within the angular span of the CME, and then provides a median speed as a proxy for overall speed. The velocity variation and minimum and maximum velocities detected are also provided for completeness.
3. Reports, forecasts and summaries of space weather[5] provided by NOAA Space Weather Prediction Centre (SWPC), which provide a discussion of solar activity, forecasts of solar and geomagnetic activity, events lists, information about solar active regions and more.
4. The Advanced Composition Explorer (ACE) list of Shocks[6] is a list of shocks observed by either the MAG or SWEPAM instruments onboard the ACE satellite.
5. The Richardson and Cane ICME list (Richardson & Cane, 2010) details interplanetary coronal mass ejections (ICMEs) identified in the near-Earth solar wind since 1996, and related back to CMEs at the Sun where possible.
6. The GOES X-ray event observations[7] identify solar flare times, locations, size and active region using data from the GOES satellites (operated by NOAA).
7. The Heliophysics Integrated Observatory (HELIO)[8] Context Service, which is a collection of solar data. It allows coronagraphs, solar images, GOES X-ray curves etc., to be plotted alongside one another for comparison, and contains movies to play simultaneously making it easier to correlate associated events.
8. The SOHO LASCO CME catalog (Yashiro, et al., 2004) provides a description of all CMEs manually identified in the LASCO coronagraphs since 1996. This includes the time

[3] http://lasco-www.nrl.navy.mil/
[4] http://sohowww.nascom.nasa.gov/
[5] http://www.swpc.noaa.gov/ftpdir/warehouse/
[6] http://www.ssg.sr.unh.edu
[7] ftp://ftp.ngdc.noaa.gov/STP/space-weather/solar-data/solar-features/solar-flares/x-rays/goes/
[8] http://www.helio-vo.eu/

of first appearance, velocity estimates, the central position angle and apparent width of the CME, as well as estimates of mass and kinetic energy.

Other sources of information for forecasters include SolarDemon[9] and the Solar Dynamics Observatory (SDO)[10], which are not discussed in any detail here as they have only become available after the time period in question. The STEREO mission[11] is also not considered in any detail in this study as it was only launched in 2006; however, it will have had some influence on determining the forecasters' opinions on whether CMEs were likely to be Earth-directed in the final few years of the interval in question.

1.2 CME PROCESSING

I began by compiling all CMEs listed in the CACTus CME archive between January 1998 and December 2009. The LASCO catalog (which is not available in real-time) is also investigated to provide a more 'definitive' dataset to compare with the CACTus results, and to identify CMEs which are missing from the CACTus catalog, to get a more complete picture. There are 9809 and 14320 CMEs in the CACTus and LASCO catalogs, respectively, in the time period in question.

All the CMEs were then studied individually to identify whether they were Earth-directed and what solar events were associated with them (i.e. flare or filament). "Earth-directed" here means that in the SWPC reports available at the time at least some component of the CME or associated shock front was expected to impact the magnetosphere, even when the CME was travelling at an angle to the Sun-Earth line. Whilst choosing front-side CMEs may appear to be a more rigorous approach than the more subjective Earth-directed, I use this approach for the intended use of these results in an operational setting. When forecasting space weather, CMEs which are clearly not directed toward the Earth are generally dismissed, and so these tables are more representative of the CMEs of interest to forecasters.

CMEs which were stated to have no earthward component or which were ignored completely in the SWPC reports were, in general, counted as non-Earth-directed. However, there are some cases where a CME was originally not discussed as having any Earth-directed component but then did have an arrival at Earth; there were 20 examples of this foundwhich are excluded from the main study, but discussed in section 2.5.

In some cases there are multiple CACTus entries for the same CME. To avoid duplication of individual CMEs the LASCO coronagraph images were studied for entries with similar lift-off times to check whether there were indeed multiple CMEs. If there were multiple CACTus entries for the same CME, the entry for which CACTus more closely matched the true angular width and position angle of the CME was used (determined by looking at the available images).

A combination of the SWPC reports, GOES X-ray lists and the HELIO context service were used to identify any associated flares and filaments. To be considered associated, the flare or filament needed to have occurred within 4 hours before the time of first appearance in the LASCO /CACTus catalog, and from a region on the solar disk close to the apparent starting location of the CME. For flares the locations was taken from the GOES X-ray list when available, otherwise the location is given as the location of the active region from which it originated. For filament eruptions the location is generally given as the centre of the filament. However, for some large filaments it is difficult to attribute the filament to a specific location, therefore the location information is currently left blank. Where a flare and filament occur close in time and location, and appear to be related, they were both considered to be associated with the CME. There are also a few occasions when the source choice was ambiguous, and so a location was not attributed to the CME.

[9] http://solardemon.oma.be
[10] http://sdo.gsfc.nasa.gov
[11] http://stereo-ssc.nascom.nasa.gov

To identify whether CMEs arrived at Earth I used a combination of the Richardson and Cane ICME list, the ACE shock list, the Kp index and the SWPC summaries between 1 and 5 days after a CME, checking for shocks and storm periods. CMEs which do not appear to strike the Earth (i.e. no shock signature identified and no apparent increase in activity within 5 days) are considered to have missed the Earth.

All events were then correlated with the maximum Kp index observed in the 24 hours following their arrival. The Kp index is used to indicate the level of geomagnetic activity. Throughout the study the storms are grouped according to Kp as classified in the NOAA Space Weather Scale for Geomagnetic storms (G-scales)[12]. Here a storm is defined as having Kp ≥ 6- which is a G2 (moderate) storm or greater on the G-scales. A G2 storm is defined as being in the range 6- ≤ Kp ≤ 6+, G3 in the range 7- ≤ Kp ≤ 7+, G4 8- ≤ Kp ≤ 9-, and G5 Kp = 9o. In the following the CMEs are discussed as having resulted in storms reaching a set value or higher, e.g., greater than Kp 6- (G2) includes all storms with Kp 6- to 9o.

Separately I compiled a list of every day for which the maximum Kp in that day reached at least Kp 6- to provide a means of checking no significant storms had been missed. The source of each of these Kp events is then identified either as one of the CMEs listed or as a result of Coronal hole activity. Coronal holes are colder regions of the solar corona where the magnetic fields are "open" allowing the solar wind to escape at a faster than average velocity. When these streams of faster solar wind hit the Earth's magnetic field they can lead to geomagnetic disturbances.

There are a few storms (13) which are attributed to CMEs which do not appear in our list, and there are also a few instances (15) when there is no obvious cause identified. This is at least in part due to data gaps in the LASCO images, which is mostly a problem in 1998-1999, but it is also known that around 19% of CMEs are not observable in LASCO (Wang, et al., 2011).

2 Results and Discussion

I found that there were 315 Earth-directed CMEs between Jan 1998 and Dec 2009 identified by this process, of which 142 (45%) caused geomagnetic storms (≥G2), and 48 (15%) caused severe geomagnetic storms where Kp reached at least 8- (G4).

In the following sections I investigate CME velocity, source location and the presence of associated flares and filaments separately, in relation to geomagnetic storm level. Ideally all the CME parameters would be studied in combination to provide more detail for a forecaster, however, the sample size of events with information on multiple parameters proves to be too small to produce robust results for any specific set of properties.

2.1 VELOCITY ESTIMATES

2.1.1 CACTus velocities

I found CACTus velocity information for 265 Earth-directed CMEs, of which 114 (43%) caused geomagnetic storms (≥G2), and 38 (14%) caused severe geomagnetic storms where Kp reached at least 8- (G4).

The CACTus median velocities cover a wide range between 139-1741 km/s. The CACTus speed is usually an underestimate as it is a median of all the detected velocities in the CME, in contrast to the LASCO catalog which is derived from tracking the leading edge of the CME, which is usually the highest speed present in a CME (Robbrecht & Berghmans, 2004). I therefore also investigate the CACTus maximum velocities, which lie between 143-2027 km/s.

[12] http://www.swpc.noaa.gov/NOAAscales/

It is important to note that the number of Earth-directed CMEs with velocity less than 500 km/s is probably underestimated. This is because these CMEs are often weak and poorly defined, and with such slow velocities they may have been considered too uninteresting to be discussed in the reports, or simply proved too difficult to robustly determine a trajectory for. However, as some CMEs with these slow velocities do appear to correlate with storms they cannot be ignored, but in practise the results in this bin are not robust.

As can be seen in Figure 1 the 500-1000 km/s bin has the largest number of Earth-directed CMEs and geomagnetic storms, for both maximum and median velocities. In the median velocities the number of Earth-directed CMEs reduces for velocities > 1000 km/s. The maximum velocities are more uniformly distributed, particularly between 500 and 2000 km/s, with a much higher number of storms in the 1500-2000 km/s bin than for the median velocity. There is a sharp drop off in velocity above 2000 km/s; it is not clear what causes this apparent saturation in maximum velocities.

The percentage of Earth-directed CMEs in each bin which led to geomagnetic storms are shown in Table 1. For both median and maximum velocities the percentage of geoeffective CMEs increases with increasing velocity up to 1500 km/s. Above this the percentage of CMEs that caused storms drops to 25% when using the median velocities, although this is based on only eight events; when looking at the maximum velocities the percentage decreases only slightly above 1500 km/s for G2 storms and increases for G3 storms and above.

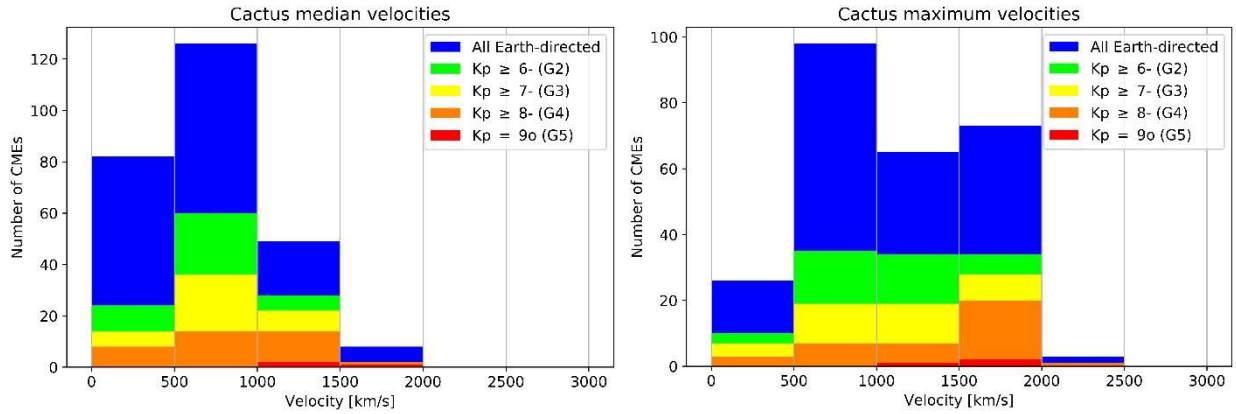

Figure 1. Plot showing the number of Earth-directed CMEs identified during the study (blue), and the numbers of these that resulted in geomagnetic storms (green to red) binned by CACTus median (left) and maximum (right) velocities.

Table 1. Percentages of Earth-directed CMEs which caused geomagnetic storms grouped by CACTus velocity estimates.

V km/s	median				maximum			
	Kp>6-	Kp>7-	Kp>8-	Kp>9o	Kp>6-	Kp>7-	Kp>8-	Kp>9o
< 500	29	17	10		39	27	12	
500-1000	48	29	11		36	19	7	
1000-1500	57	45	29	4	52	29	11	2
1500-2000	25	25	25	12	47	39	27	3
2000-2500					33	33	33	

The CACTus data can be combined to provide a more detailed picture of how the CACTus velocity estimates affect geoeffectiveness. Figure 2 shows the percentage of Earth-directed CMEs that caused geomagnetic storms of increasing intensity in bins of median and maximum CACTus estimates. It is important to note that some bins have very few Earth-directed CMEs (number of

CMEs in each bin is shown in Figure 3), particularly for maximum velocities greater than 2000 km/s, so the percentages may be not be particularly meaningful.

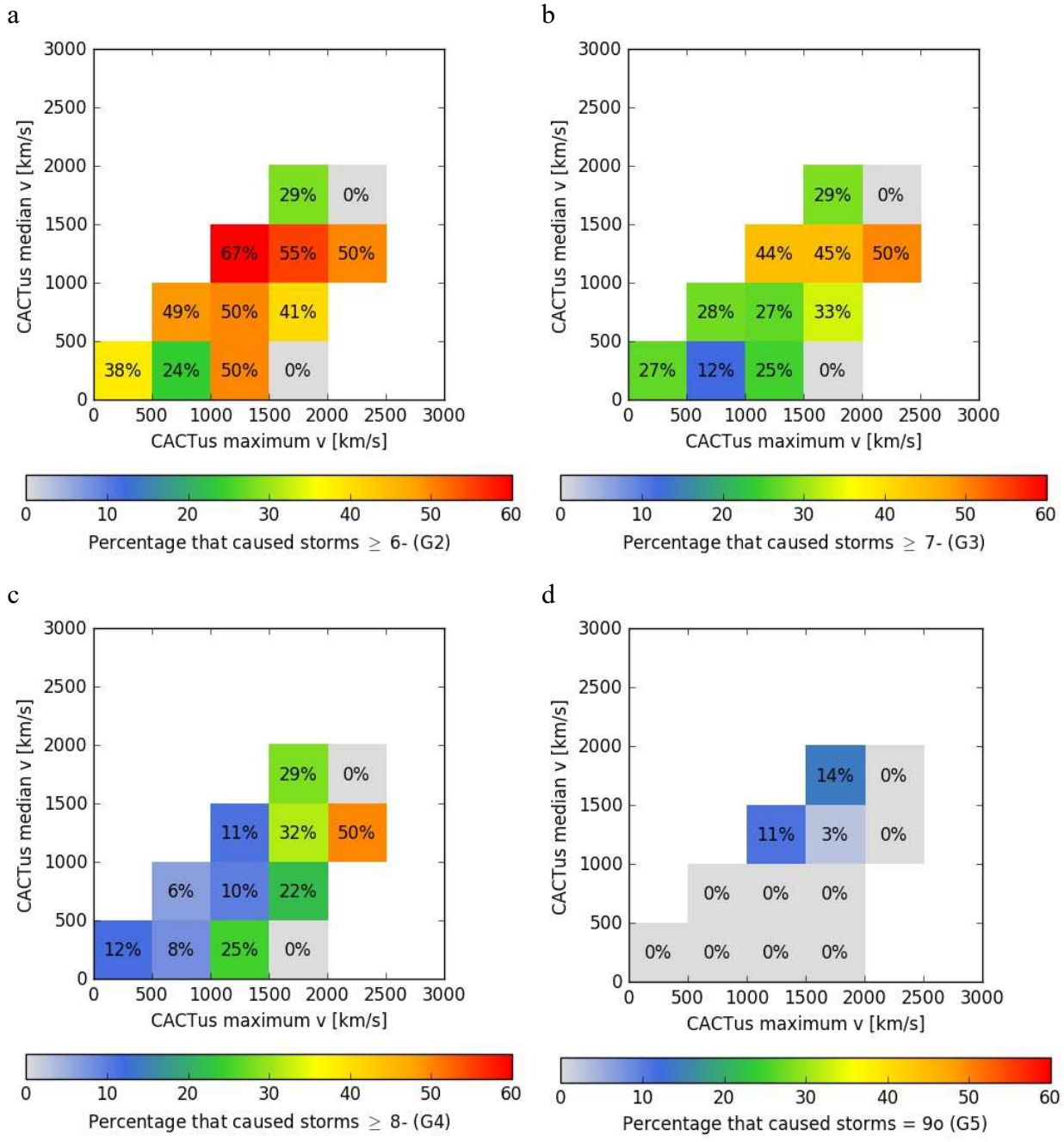

Figure 2. Percentages of Earth-directed CMEs which caused geomagnetic storms binned according to CACTus median and maximum velocities for storms with Kp ≤ 6- (a), Kp ≤ 7- (b), Kp ≤ 8- (c) and Kp = 9o (d).

The highest percentage of storms (≥G2) occurs when both median and maximum velocities are in the range 1000-1500 km/s. The only Kp 9o events occur for CMEs which CACTus has provided both maximum and median velocities greater than 1000km/s. Whilst the percentages are low (between 3-12% for the three bins) this may mean we are able to have some confidence that CMEs with velocity estimates less than 1000 km/s will not lead to Kp 9o storms.

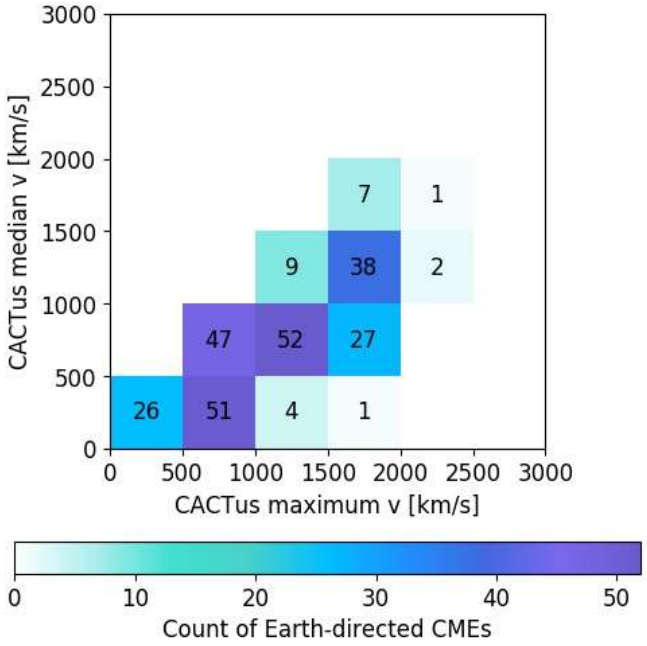

Figure 3. Count of Earth-directed CMEs in bins of CACTus median and maximum velocity.

2.1.2 LASCO velocity estimates

CME linear velocity estimates from the LASCO catalog are produced manually, well after the event, and can be considered to be a more 'definitive' dataset than CACTus. Whilst they are not available in near real-time, most studies use these velocities for their analysis, and the CACTus velocity estimates are known to differ significantly from the LASCO catalog (Robbrecht & Berghmans, 2004), so it is useful to analyse the LASCO velocity estimates for comparison.

Using the LASCO catalog I found velocity information for 310 CMEs for the time period considered, 140 (45%) of which caused storms ≥ G2 and 48 (15%) caused storms ≥ G4. The LASCO velocities have a range of 179-3387 km/s, with an average (median) of 1015km/s (916km/s), which is consistent with analysis by Gopalswamy, et al., (2007) who found an average of 933km/s for on disk halo CMEs, and 1421km/s for limb halo CMEs in between 1996 and 2005. Zhang, et al. (2007) presented a range of around 60-2800km/s with a mean (median) of 945km/s (875km/s) for CMEs during 1996-2005. The differences in the range are in part due to the selection criteria and time span investigated, and in part due to their figures only including those CMEs deemed to have caused storms. When only those CMEs that caused storms (Kp ≥ 6-) are included, the range in velocities is 206-2861km/s and the mean (median) increases to 1100km/s (973km/s).

Figure 4 shows the number of Earth-directed CMEs in 500km/s velocity bins, and the count in each bin that caused storms. Most Earth-directed CMEs have velocities of 500-1000 km/s (a total of 121 events), and CMEs in this velocity bin also caused the largest number of geomagnetic storms (52 with Kp ≥ 6-). The percentage of CMEs that caused a geomagnetic storm increased with velocity (Table 2), up to 83% for CMEs with velocities in the range 2500-3000km/s. However, the likely statistical significance of events with the highest velocities is low due to the small number (only 7 events) of Earth-directed CMEs with velocity greater than 2500km/s. Kp 9o events only occur for velocities greater than 1500 km/s, which is in agreement with findings by Srivastava & Venkatakrishnan (2004) who found that CMEs with velocities greater than 1500 km/s can cause superintense storms (based on Dst < -200nT).

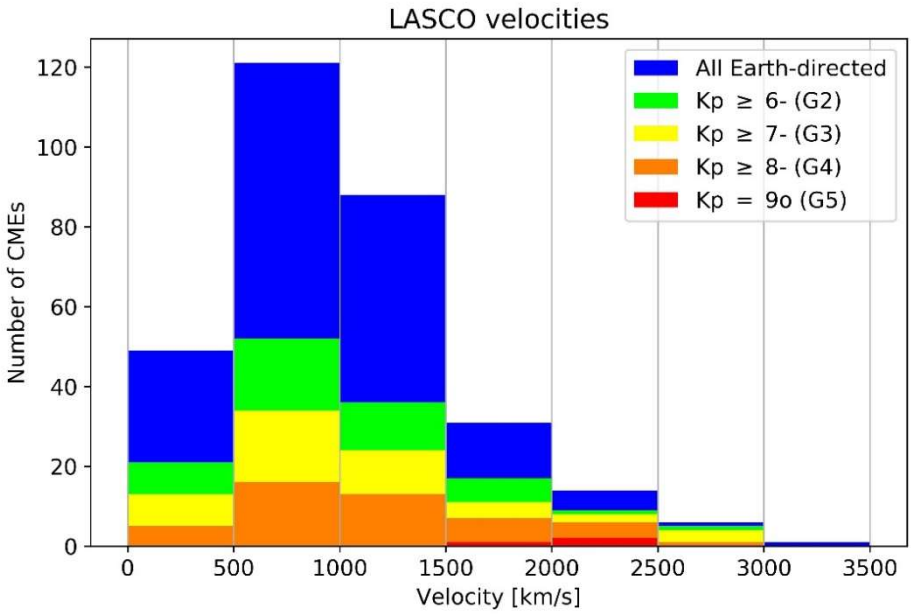

Figure 4. Total number of Earth-directed CMEs identified during the study (blue), and the numbers of these that resulted in geomagnetic storms (green to red), for Kp of 6-to 9o (G2-G5), binned by LASCO velocities. Note the number of Earth-directed CMEs in the 0-500km/s bin is likely to be underestimated (see text).

Table 2. Percentage of Earth-directed CMEs causing a geomagnetic storm based on 500 km/s bins of LASCO velocity estimates.

V km/s	Kp > 6-	Kp > 7-	Kp > 8-	Kp > 9o
< 500	43	27	10	
500-1000	43	28	13	
1000-1500	41	27	15	
1500-2000	55	36	23	3
2000-2500	64	57	43	11
2500-3000	83	67	17	

The LASCO catalog provides more velocity estimates greater than 2000 km/s for Earth-directed CMEs than in the CACTus analysis. The percentage of CMEs that lead to geomagnetic storms for the bins of velocity is broadly similar to the CACTus maximum velocities, but the percentages continue to increase above 2000 km/s up to 83%, which is a much higher percentage of geoeffectiveness than for any of the CACTus velocity bins. The velocities associated with storms of Kp = 9o are higher for LASCO (> 1500 km/s) than CACTus (> 1000 km/s, both median and maximum velocities).

2.2 CME SOURCE LOCATION

The source location is a major factor determining if a CME will be directed towards the Earth. In this study the source location is considered to be the same as the location of observed flare/filaments site as this information is most readily available when producing a forecast. Some studies have suggested this may not be the best way to identify location (e.g. Moon, et al., 2009; Wang, et al., 2002), as this can differ from the apparent origin of the CME in the LASCO images. This difference may be caused by projection effects, or that CMEs may not propagate radially with respect to their source location (Plunkett, et al., 2001), or they may be deflected by interaction with the ambient corona (Cremades & Bothmer, 2004; Wang, et al., 2011).

As discussed in Section 1.2 there is some uncertainty in identifying the source location for some CMEs; of the 315 Earth-directed CMEs in this work, source locations have been identified for 302.

The count of Earth-directed CMEs binned by heliolongitude is shown in Figure 5, and the percentage in each bin that caused a storm is shown in Table 3. Approximately 30% (97) Earth-directed CMEs originate between ±15º longitude, with more CMEs considered to be Earth-directed in the western hemisphere (172) than the east (126), and four CMEs which were located directly on the central meridian. Skirgiello (2005) also found a persistent predominance of CMEs in the western hemisphere, which may be due to some instrumental or observational bias, or potentially caused by the geometry of asymmetrically shaped CMEs.

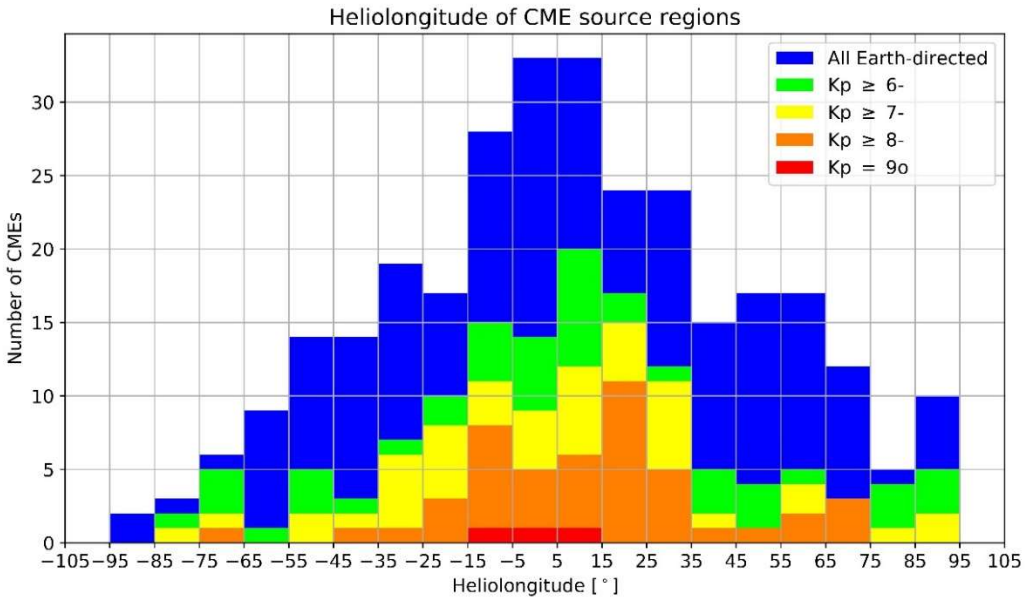

Figure 5. Count of Earth-directed CMEs binned by heliolongitude of the associated flare or filament.

Table 3. Percentage of Earth-directed CMEs, from 10º longitude bins, that caused a geomagnetic storm with Kp 6- or more.

longitude	Kp ≥ 6-	Kp ≥ 7-	Kp ≥ 8-	Kp = 9o
-95 to -85				
-85 to -75	67	33		
-75 to -65	83	33	17	
-65 to -55	11			
-55 to -45	35	14		
-45 to -35	21	14	7	
-35 to -25	37	32	5	
-25 to -15	59	47	18	
-15 to -5	54	39	29	4
-5 to 5	42	27	15	3
5 to 15	61	36	18	3
15 to 25	71	63	46	
25 to 35	50	46	21	
35 to 45	33	13	7	
45 to 55	24	6	6	
55 to 65	29	24	12	
65 to 75	25	25	25	
75 to 85	80	20		
85 to 95	50	20		

CMEs in the western hemisphere (particularly heliolongitudes of 5º - 25º) are also more likely to cause storms than other from other source longitudes, which is consistent with previous studies (e.g. Kim et al., 2005; Zhang et al., 2007). However, the largest storms (Kp = 9o) follow CMEs from the central 30º, which is consistent with Gopalswamy et al. (2007), who found that the overall strength of geomagnetic storms decreased as the solar source location changes from the centre to the limb. It is also worth noting that CMEs occurring on the limbs (|>60º|) which are wide enough to have an Earth-directed component also have an increased chance of causing storms. Shen, et al., (2014) noted that limb CMEs can become geoeffective if they have a large angular width.

In latitude (Figure 6), the Earth-directed CMEs are distributed approximately symmetrically about the equator (150 north, 149 south and 3 on the equator). The ±5-15º bins have the most Earth-directed CMEs, 80 in the south and 69 in the north.

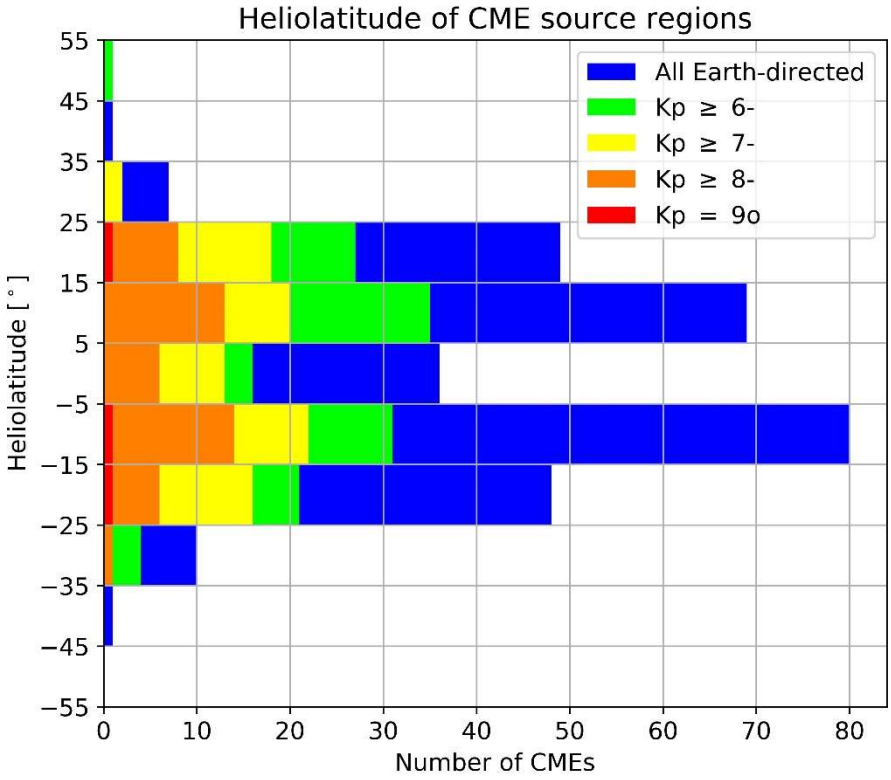

Figure 6. Count of Earth-directed CMEs binned by heliolatitude of the associated flare or filament (blue) and the count in each bin that caused storms of Kp ≥ 6- (green) through to Kp = 9o (red).

Wang et al., (2011) identified a peak occurrence of CMEs between 15º-30º, with very few CMEs originating equatorwards of 15º latitude. This discrepancy between their findings and Figure 6 is likely to be due to the method of defining the source location. Wang et al., (2011) defined the source as the centre of the eruption feature identified in the SOHO/EIT images, then converted the apparent coordinates to heliographic coordinates.

All the Earth-directed CMEs were within ±55º and all but three were within ±35º heliolatitude. Table 4 shows the percentage of Earth-directed CMEs that caused geomagnetic storms in each bin of latitude. The most geoeffective bin is 15-25º in the northern hemisphere where 55% of Earth-directed CMEs caused a storm during which Kp reached at least 6-. The 100% value for the 45-55º bin is not statistically significant as this is based on only a single event.

Table 4. Percentage of Earth-directed CMEs, from 10º heliolatitude bins, that caused a geomagnetic storm with Kp 6- or more.

Latitude	Kp ≥ 6-	Kp ≥ 7-	Kp ≥ 8-	Kp = 9o
45 to 55	100			
35 to 45				
25 to 35	29	29		
15 to 25	55	37	16	2
5 to 15	51	29	19	
-5 to 5	44	36	17	
-15 to -5	39	28	18	1
-25 to -15	44	33	13	2
-35 to -25	40	10	10	
-45 to -35				
-55 to -45				

The analysis of latitude and longitude of source locations combined can provide more information about the likelihood of causing geomagnetic storms of different magnitudes. Figure 7 shows the number of Earth-directed CMEs in each latitude/longitude bin and gives a sense of how meaningful the percentages are for each bin (note the bin sizes are increased compared to earlier figures to provide a higher count in each bin). For instance, near the limbs there are at most only four CMEs in any of the bins, so the percentages here are unlikely to be robust.

Figure 8 shows the percentage of CMEs in each bin which caused storms with Kp ≥ 6- (a) up to Kp = 9o (d). The small sample (3 events) of Kp 9o storms only occur from CMEs located at central longitudes and ± 10-30º latitude. The highest percentage of G4 storms follow CMEs from the block 10º-30º west and central latitudes.

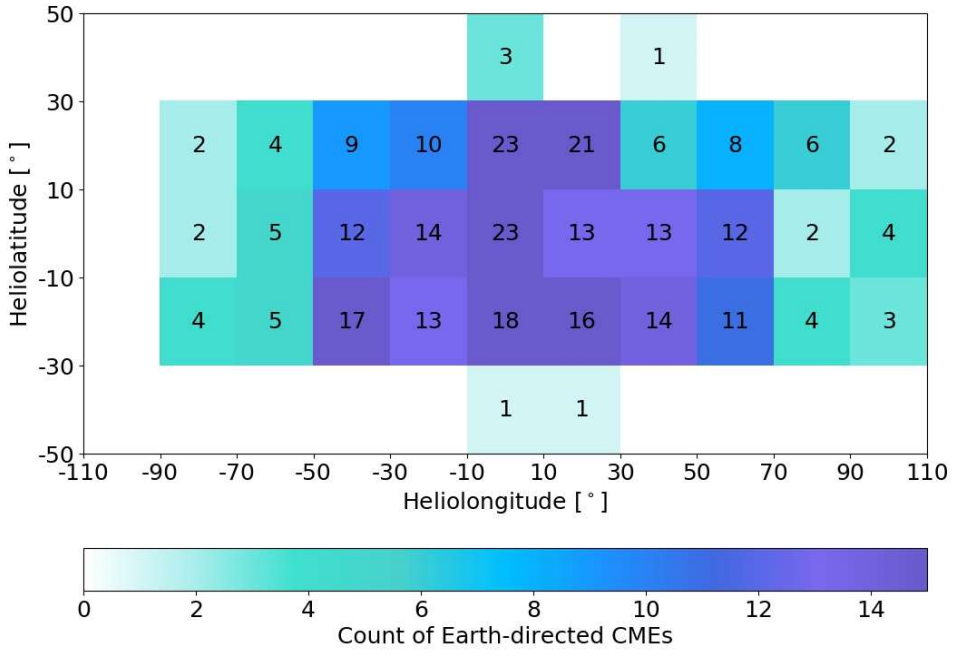

Figure 7. Total count of Earth directed CMEs Jan 1998-Dec 2009 binned by source region latitude and longitude.

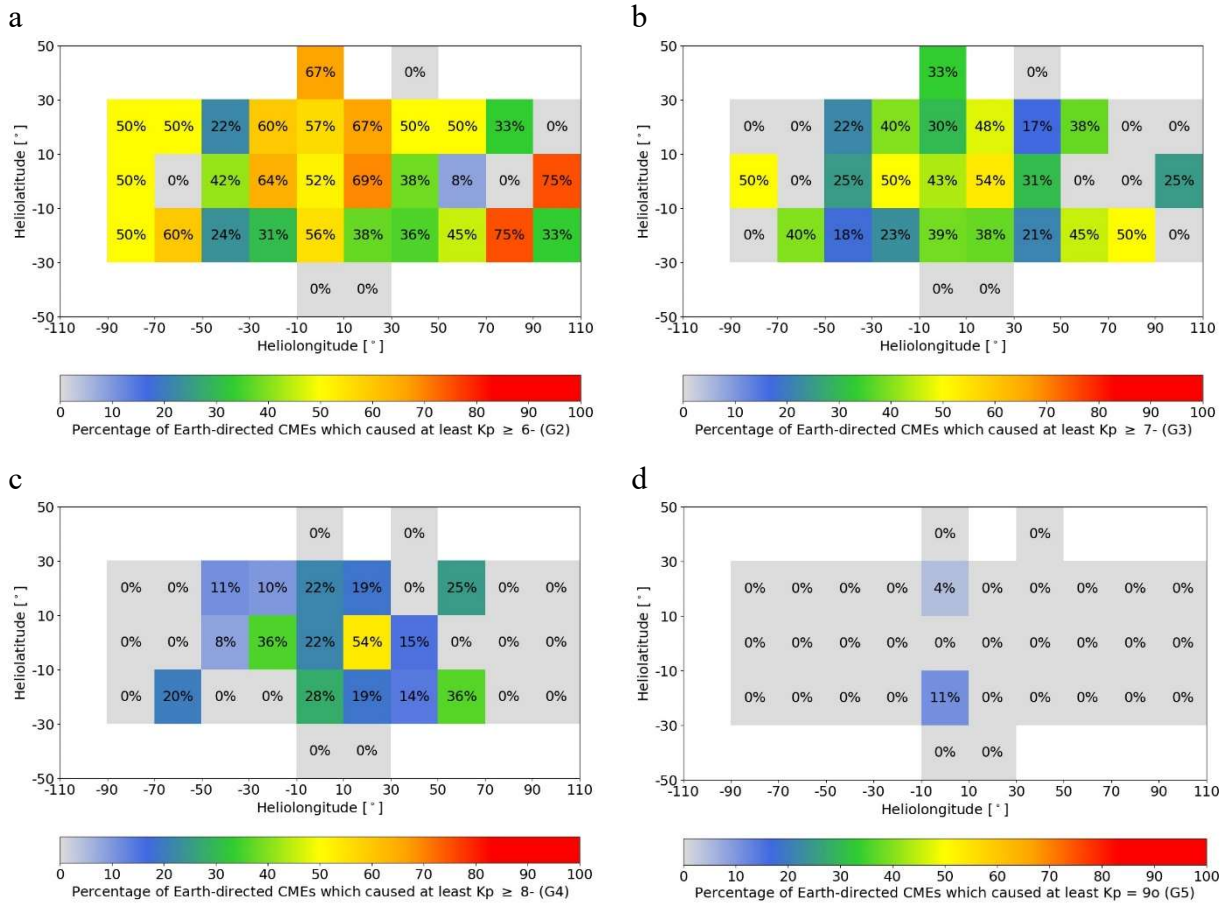

Figure 8. Percentages of Earth-directed CMEs Jan 1998-Dec 2009 which caused geomagnetic storms binned by source region latitude and longitude, for storms with Kp ≤ 6- (a), Kp ≤ 7- (b), Kp ≤ 8- (c) and Kp = 9o (d).

2.3 ASSOCIATED FLARES AND FILAMENTS

In total there are 250 flares and 39 filaments associated with Earth-directed CMEs in this study; there were also 23 occasions when a CME was associated with both a flare and filament, which occurred close in time and appear to be related, and 3 occasions when no flare or filament could be clearly associated with the CME. Solar flares are classified based on the peak flux in Watts per square metre of X-rays with wavelengths 100 to 800 picometre. The classification uses the letters A (< 10^{-7}W/m^2), B (10^{-7}-10^{-6} W/m^2), C (10^{-6}-10^{-5} W/m^2), M (10^{-5}-10^{-4} W/m^2) and X (>10^{-4} W/m^2), and is based on measurements made by the GOES spacecraft.

Table 5 shows the percentage of Earth-directed CMEs associated with each of these sources (flares separated by class) that caused geomagnetic storms.CMEs associated with X-class solar flares caused the highest percentage of geomagnetic storms, with 64% leading to Kp 6- or above. CMEs associated with X-class flares were also the only CMEs to lead to Kp 9o events.

Table 5. Table showing the percentages of Earth-directed CMEs associated with different classes of flares and filaments that caused geomagnetic storms. The total column is the total number of Earth-directed CMEs associated with each type of flare/filament.

	Total	Kp ≥ 6-	Kp ≥ 7-	Kp ≥ 8-	Kp = 9o
X-class	61	64%	51%	25%	5%
M-class	120	41%	23%	14%	
C-class	62	44%	33%	16%	
B-class	7	29%	29%	14%	
filament + flare	23	44%	32%	16%	
filament only	39	31%	13%	3%	

For Kp ≥ 6- events the percentages for the other classes of flare are similar. However, it is important to note that there are only seven examples of Earth-directed CMEs related to B-class flares. M-class flares had the most examples but lower percentages for all storm levels than C-class flares.

X and M-class flares are generally considered to be most geoeffective, as larger flares release more energy and could therefore be expected to be associated with larger CMEs. CMEs associated with B-class flares may be considered less likely to cause storms and could therefore be less likely to be reported, just as CMEs related to M-class flares may be reported more readily than either B- or C-class flares. However, other studies have shown that the strength of a geomagnetic storm does not appear to be related to the magnitude of flares, and flare size on its own is, therefore, not reliable for prediction (e.g., Srivastava & Venkatakrishnan, 2004; Zhang et al., 2007).

CMEs associated with filament eruptions have lower percentages for all storm categories. This is consistent with previous studies which showed that flares have a stronger association with geoeffective CMEs than filaments (e.g., Srivastava & Venkatakrishnan, 2004; Wang, et al., 2002).

2.4 ACCOUNTING FOR COMBINED CMES

Up to this point if multiple CMEs combined en route to the Earth, resulting in a single storm they have each been counted as being individually geoeffective, but that is perhaps misleading. Stating that a CME with a certain velocity and from a particular longitude caused a storm of a set size is not entirely true if the storm actually resulted from the combination of several CMEs. Some authors (e.g., Wang, et al., 2002) deal with this by attributing all effects to the first CME, but that may also be misleading if that first CME is overtaken, for example.

In our analysis, Kp values are attributed to the first CME, if that CME gives rise to a storm level Kp before an distinct second CME arrival. Geomagnetic activity after that second CME arrival is considered to result from the CMEs in combination, and these CMEs are excluded from this section of the study. If the arrivals are not clearly separated, are close together (<12 hours), or the CMEs are thought to have combined in transit then the CMEs are counted as ‘combined’ and are also excluded in this section. This resulted in 47 CMEs being excluded from this part of the study, leaving 268 CMEs.

The Kp 9o events are still counted separately in this definition; although the storm in Oct 2003 was two events in two days, the shock arrivals are far enough apart (more than 24hrs) that it is reasonable to suggest both CMEs resulted in Kp 9o, although arguably the magnetic field was already disturbed for the second CME arrival.

Excluding these combined events does not make a significant difference to the velocity analyses. In general there is a slight reduction in the percentages in each bin, with the only exception being in the CACTus analysis where the percentage of G5 events increases from 14 to 20 when both the median and maximum velocities are above 1500 km/s. This is due to the total number of Earth-directed CMEs in that bin reducing from 7 to 5.

In latitude there is again an overall reduction in the percentages of CMEs that caused storms when removing combined CMEs from the selection. The most significant difference is that the percentage of Earth-directed CMEs that lead to G4 events from the central bin dropped from 17 to 0 percent.

Removing the combined CMEs makes more of a difference to the heliolongitude plot, shown in Figure 9, particularly between 5º-25º degrees west, where there is a clear reduction in storms (and therefore total CMEs). In total there are still more Earth-directed CMEs in the western hemisphere but the difference between the hemispheres is slightly reduced, with 141 CMEs originating in the

west and 110 in the east. There is also a noticeable reduction in the number of storms between 35º-55º in both the east and west hemispheres.

When the latitude and longitude are combined, as in Figure 10, the percentages are in general smaller. The percentage of CMEs resulting in Kp 9o increases, but this is probably an artefact of the total number of CMEs in those bins being reduced.

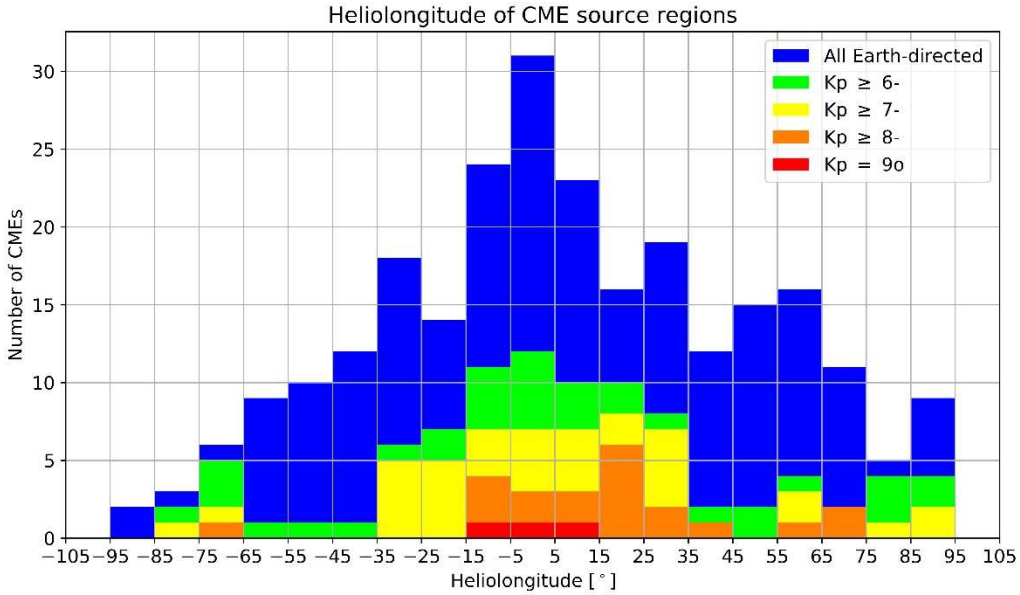

Figure 9. Count of Earth-directed CMEs that did not combine with other CMEs, binned by heliolongitude of the associated flare or filament (blue) and the count in each bin that caused storms of Kp ≥ 6- (green) through to Kp = 9o (red).

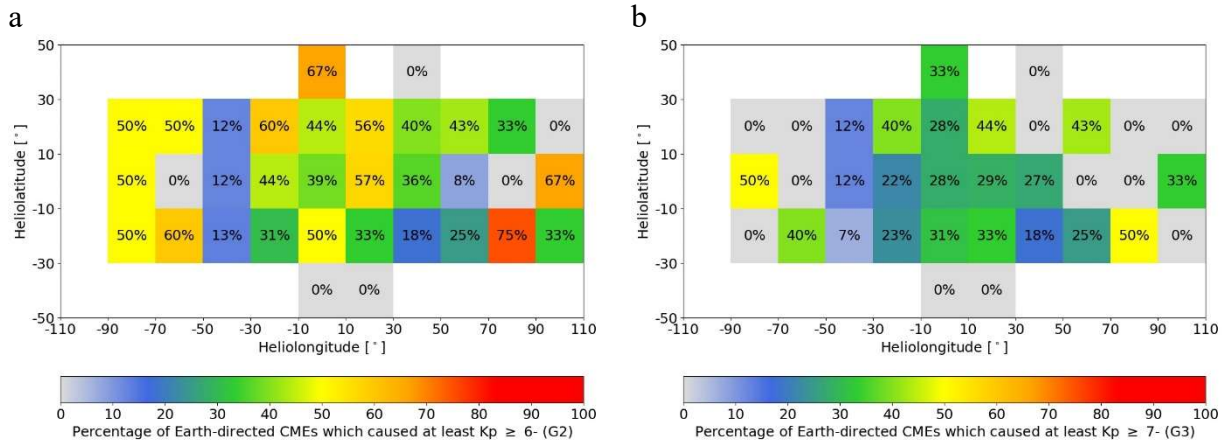

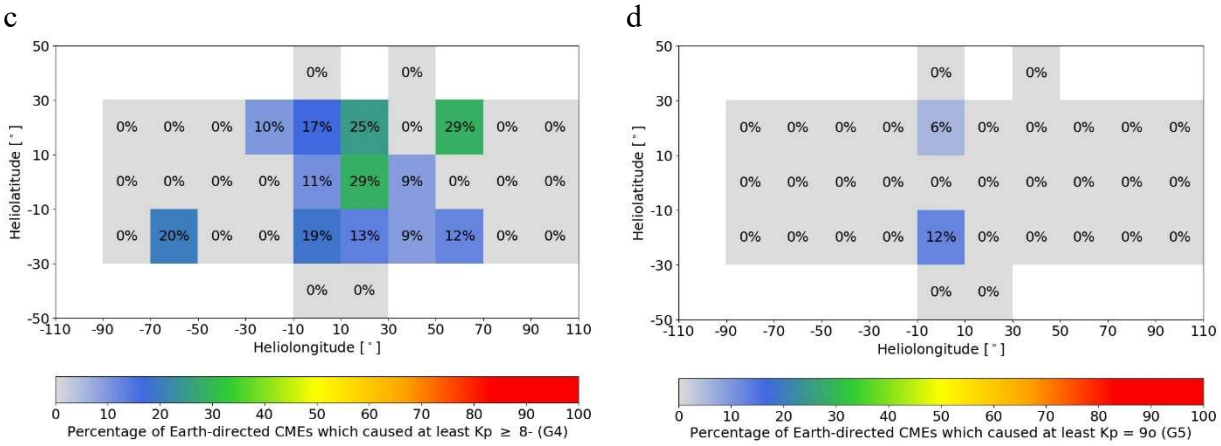

Figure 10. Percentages of Earth directed CMEs Jan 1998-Dec 2009 that did not combine with other CMEs, that resulted in geomagnetic storms binned by source region latitude and longitude. For storms with Kp ≥ 6- (a), Kp ≥ 7- (b), Kp ≥ 8- (c) and Kp = 9o (d).

There were 21 events (47 CMEs in total) resulting from CMEs in combination (2 or more arriving close together or combining in the heliosphere) so it is difficult to draw any robust conclusions about specific parameters. However, 100% of these events caused at least Kp 5- (G1), 95% lead to G2 storms, and 53% lead to G4 storms (> Kp 8-). Gopalswamy et al. (2007) found the most intense storms occur when there are successive CMEs and Schwenn et al. (2005) noted that the effects of CMEs which interact and merge are highly unpredictable.

2.5 UNEXPECTED GEOEFFECTIVE CMES

As mentioned in section 1.2 there were a few occasions when CMEs were not originally thought to be Earth-directed, but did then have an arrival at Earth; 20 such CMEs were identified. The number of these CMEs for each range of K values is shown in Table 6. 80% of those CMEs that arrived caused only minor geomagnetic activity (< G2); of the rest there was a range of resultant Kp, with one of these CMEs causing Kp ≥ 8-, which is a significant level of activity for a CME that was not expected to hit the Earth. CME source location was only found for 8 of the 20 examples, 6 of which originated in the eastern hemisphere. This may be a further indication of observational bias (mentioned in 2.2), as CMEs in the eastern hemisphere are considered to be less likely to be geoeffective.

Table 6. Number of CMEs that were originally not expected to become geoffective that did then arrive at Earth

	Number of CMEs	Percentage
Kp < 6-	16	80%
6- ≤ Kp < 7-	3	15%
7- ≤ Kp < 8-	1	5%
8- ≤ Kp < 9-	1	5%
Kp = 9o	0	0%

2.6 SOURCES OF GEOMAGNETIC STORMS

As part of the analysis I looked at all occasions within the time period when Kp reach 6- or more and, where possible, identified the source of the disturbance. This allowed us to check where CMEs might have been missed but also identified occasions when geomagnetic storms were related to other features, such as coronal holes. This process identified 290 storms during the period in question, 163 of which were related to CMEs, 111 to coronal holes (CH) and 16 for which the source could not be identified. Figure 11 to Figure 14 show the number of storms between 1998 and 2009 for each level of Kp separated by their solar sources. Also plotted is the sunspot number to provide an indication of the solar cycle.

In general coronal holes caused lower levels of activity than CMEs with only 1 event at G4 resulting from a coronal hole. CMEs also caused more storms at G3 and above for all years; at G2 there were two years when coronal holes caused more storms than CMEs.. This is most notable in 2003 during the descending phase of the solar cycle; during this phase there are many large, near-equatorial coronal holes and equatorward extensions of the polar coronal holes (e.g. Hundhausen, et al., 1981, Feynman & Gu, 1986).

The number of storms appears to increase towards the maximum in the solar cycle (~2000) but there is no clear reduction in the number of storms during the descending phase, until the solar minimum (2007-2009). Ideally the analysis would include multiple solar cycles to identify recurring patterns. Unfortunately, many of the data sources used in this study are only available from 1998, and we are currently just over half way into the next solar cycle.

It is important to note that geomagnetic storms, including the most intense storms, are not confined to solar maximum.

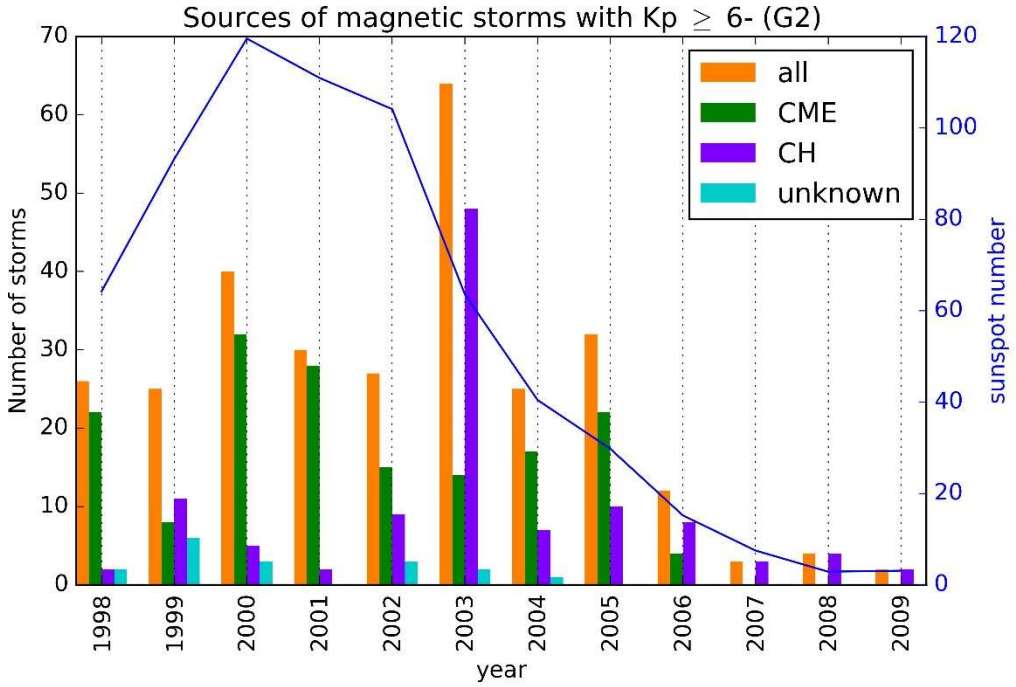

Figure 11. Number of storms per year that lead to Kp ≥ 6- between 1998 and 2009 separated by source type (total number in orange). Also shown is the average yearly sunspot number (blue line) to provide an indication of the solar cycle.

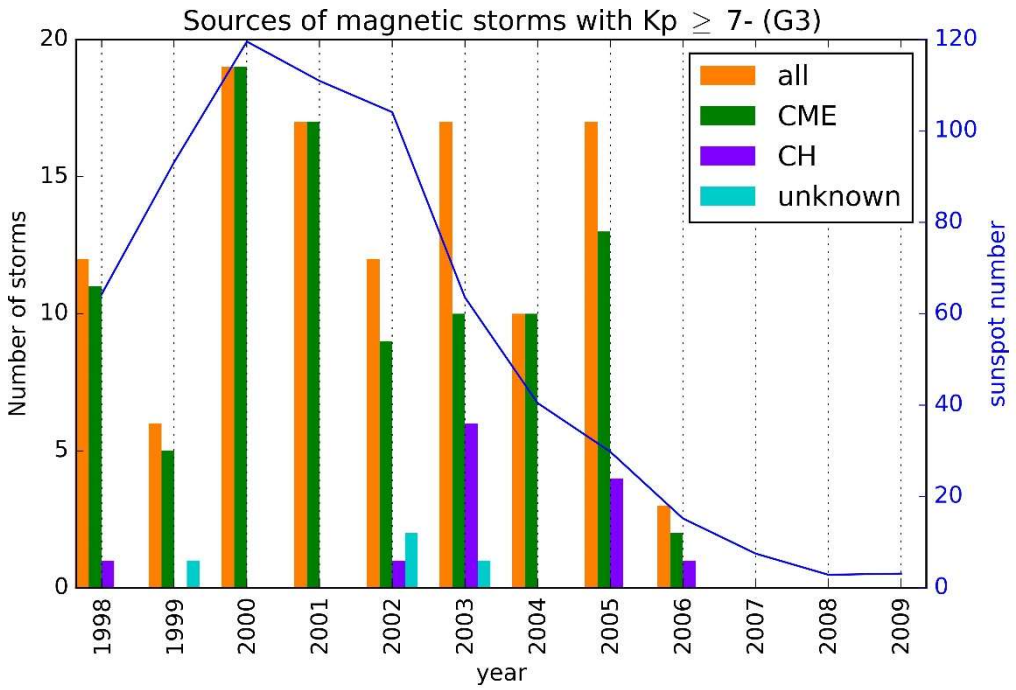

Figure 12. As Figure 11 for all storms with Kp ≥ 7-.

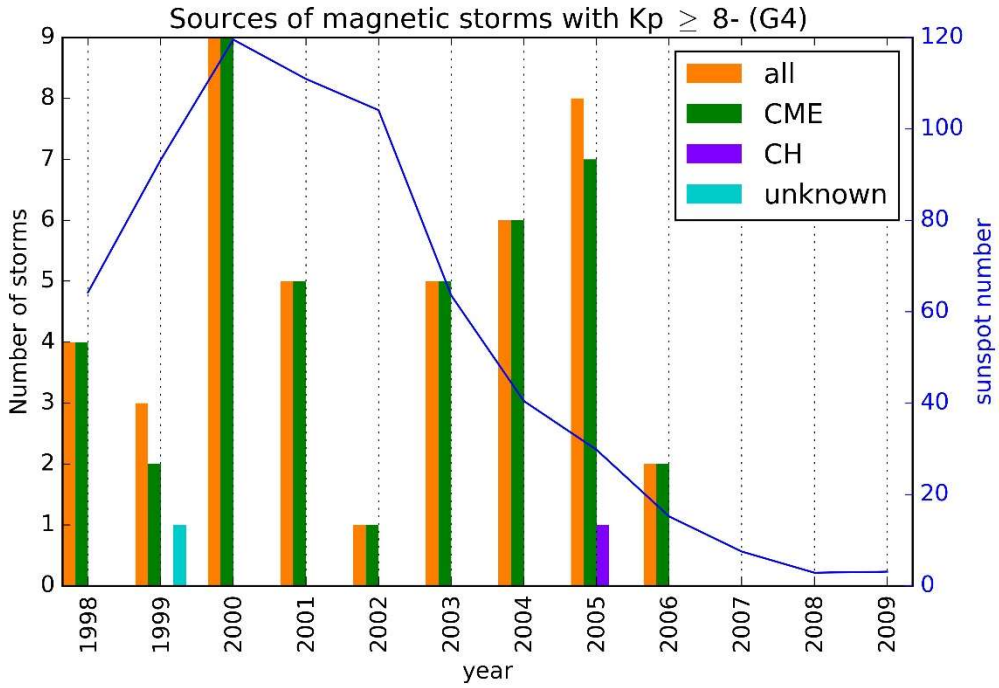

Figure 13. As Figure 11 for all storms with Kp ≥ 8-.

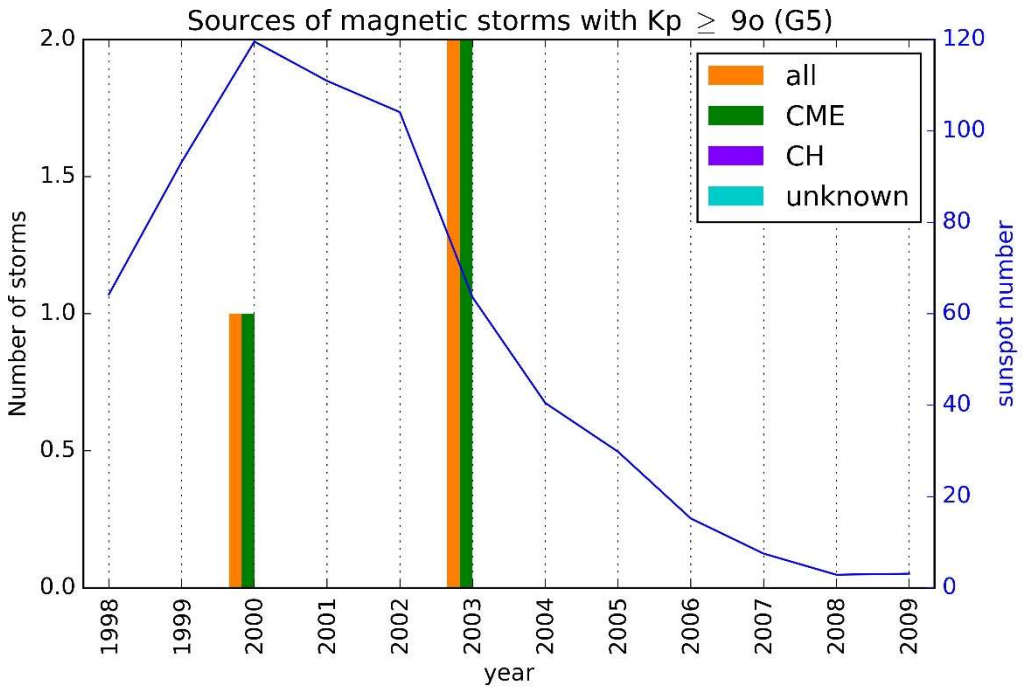

Figure 14. As Figure 11 for all storms with Kp = 9o.

3 Summary

This study analysed properties of Coronal Mass Ejections (CMEs) during a 12 year period from Jan 1998 to Dec 2009. The aim is to provide operational forecasters with guidance on the likely geoeffectiveness of a given CME based on the data that are available in near real-time. The main results of this study are:

1. CME velocity can be a useful indicator of CME geoeffectiveness particularly when using the LASCO velocities. However, G4 storms occurred for all velocities, so even slow CMEs cannot be ignored.
2. The real-time estimates of velocity from CACTus differ substantially from the LASCO catalog, although there is still a general increase in the percentage of CMEs that resulted in storms with increasing CACTus velocity. This is an important point for real-time forecasting as comparing a real-time velocity estimate from CACTus with a table of percentages based on the LASCO catalog could yield an incorrect expectation of a storm occurring.
3. Combining the median and maximum velocity estimates from CACTus can provide a useful tool for estimating the geoeffectiveness of CMEs. For example, Kp 9o events occur only for CMEs where both the median and maximum velocities are greater than 1000km/s.
4. In terms of the longitude of the source region there is a clear western bias, both in Earth-directed CMEs and those that became geoeffective. Kp 9o events occur only from the central 20º, but the possibility of storms from limb events (particularly from the west limb) cannot be dismissed.
5. There are two distinct bands of Earth-directed CMEs at 5º-15º heliolatitude approximately symmetric about the equator. CMEs originating from heliolatitudes within ±25º are most likely to cause geomagnetic storms.
6. CMEs associated with filament eruptions are less geoeffective than those associated with flares, in agreement with other studies (e.g., Wang et al., 2002; Srivastava & Venkatakrishnan, 2004).
7. CMEs associated with X-class flares were the only ones to result in Kp 9o events, and had the highest percentage of all levels of storm. The percentages for CMEs associated with B,

C and M-class flares are much more similar, which would suggest that below X-class, the flare size does not make a considerable difference to geoeffectiveness, which is consistent with other studies (e.g., Srivastava & Venkatakrishnan, 2004; Zhang, et al., 2007)

Ideally all the parameters available would be combined to provide the maximum information about the geoeffectiveness of a CME for forecasters. Under certain circumstances we can provide more detailed statistics, for example, there are 25 examples of Earth-directed CMEs with CACTus median velocity between 500-1000km/s and CACTus maximum velocity of 1000-1500km/s associated with an M-class solar flare, 28% of which resulted in a storm of Kp≥6-. However, when CMEs are separated into such specific parameter groups the number of CMEs is not sufficient for statistically significant results. In the above example if we replace the M-class flare with an X-class flare the number of Earth-directed CMEs drops to only 10 instances, and if we introduce the source longitude to either example that number drops further, even for the central bin where there are most examples in Figure 7 (2 X-class flares and only 7 M-class flares). In future work we intend to populate the database with more CMEs (i.e. 2010 and beyond) which will help to increase the number of examples, but it could be many years before there are enough Earth-directed CMEs to make all the parameter groups statistically significant.

It is also important that one of the most important factors in determining how geoeffective a CME will be is the orientation of the magnetic field within the CME. For example, in previous studies, around 15-20% of Magnetic Clouds (one of the types of ICME signature) had fully northward axial field (Lepping, et al., 2006; Gopalswamy, et al., 2007), and therefore were not as geoeffective as if they had southward field. However, we still cannot determine the orientation satisfactorily until it arrives at ACE (or more recently the DSCOVR satellite), and so the orientation of the magnetic field within the CME is not considered in this study, which is based primarily on forecasting further ahead than the warning provided by satellites at the L1 point.

The ambient conditions of the heliosphere at the time of a CME will also have an effect on the geoeffectiveness of CMEs, but that is beyond the scope of this study. Until there are reliable physical models of the heliosphere it is hard to quantify this effect on the CME-storm relationship.

Glossary

Coronal Hole. A region in the Sun's outer atmosphere (corona) where hot material can flow unrestrained by its magnetic fields out into space.

Coronal Mass Ejection or CME. The eruption of a portion of the outer atmosphere of the Sun into space, caused by rapid changes in its magnetic field. Often occurs along with a solar flare.

Filament. When the Sun is viewed in H-alpha (121.6mm) filaments can be seen as long and narrow dark features. They are clouds of ionized gas suspended above the Sun's surface between magnetic regions of opposite polarity. When a solar filament becomes unstable it may erupt into space leading to a coronal mass ejection.

Geoeffective. If an event on the Sun has a measureable impact at Earth, causing geomagnetic activity it is considered to be geoeffective.

Halo CME. A Coronal mass ejection which can be seen in coronagraph imagery to extend in all directions around the Sun (i.e. 360 degree angular width).

High Speed Stream. A fast moving stream of solar wind, responsible for magnetic storms, usually associated with coronal holes.

Kp index. A global measure of geomagnetic activity based on the K-index at 13 sub-auroral magnetic observatories. The K-index is a quasi-logarithmic scale that is a measure of the maximum

range in the horizontal component of the magnetic field at an observatory in a 3-hour time window.*Solar Flare.* Energy released by the explosive reorganisation of magnetic fields within the Sun's atmosphere.

Solar Wind. The ever-present expansion of the Sun's hot outer atmosphere into the solar system, which carries space weather within it.

References

Arge, C. N. et al., 2004. Stream structure and coronal sources of the solar wind during the May 12th, 1997 CME. *Journal of Atmospheric and Solar-Terrestrial Physics,* Volume 66, pp. 1295-1309.

Arge, C. N. & Pizzo, V. J., 2000. Improvement in the prediction of solar wind conditions using near-real time solar magnetic field updates. *J. Geophys. Res.,* Volume 105, pp. 10465-10480.

Brueckner, G. E. et al., 1998. Geomagnetic storms caused by coronal mass ejections CMEs: March 1996 through June 1997. *J. Geophys. Res.,* Volume 25, pp. 3019-3022.

Cane, H. V., Richardson, I. G. & St. Cyr, O. C., 2000. Coronal mass ejections, interplanetary ejecta and geomagnetic storms. *Geophys. Res. Lett.,* 27(21), pp. 3591-3594.

Cremades, H. & Bothmer, V., 2004. On the three-dimensional configuration of coronal mass ejections. *Astron. astrophys.,* Volume 422, pp. 307-322.

Cremades, H. & St. Cyr, O. C., 2007. Coronal mass ejections: solar cycle aspects. *Adv. Space Res.,* pp. 1042-1048.

Feynman, J. & Gu, X. Y., 1986. Prediction of geomagnetic activity on time scales of one to ten years. *Reviews of Geophysics,* 24(3), pp. 650-666.

Gopalswamy, N. et al., n.d. Intensity variation of large solar energetic particle events associated with coronal mass ejections. *J. Geophys. Res.,* Volume 109, p. A12105.

Gopalswamy, N., Yashiro, S. & Akiyama, S., 2007. Geoeffectiveness of halo coronal mass ejections. *J. Geophys. Res.,* Volume 112, p. A06112.

Hundhausen, A., Hansen, R. & Hansen, S., 1981. Coronal evolution during the sunspot cycle: coronal holes observed with the Mauna Loa K-Coronameters. *J. Geophys. Res.,* 86(A4), pp. 2079-2094.

Kim, R.-S.et al., 2010. An empirical model for prediction of geomagnetic storms using initially observed CME parameters at the Sun. *J. Geophys. Res.,* p. A12108.

Kim, R.-S.et al., 2005. Forecast evaluation of the corona mass ejection (CME) geoeffectiveness using halo CMEs from 1997 to 2003. *J. Geophys. Res.,* Volume 110, p. A11104.

Lepping, R. P. et al., 2006. A summary of WIND magnetic clouds for years 1995-2003: model-fitted parameters, associated errors and classigfications. *Ann. Geophys.,* Volume 24, pp. 215-245.

Moon, Y.-J., Kim, R.-S. & Cho, K.-S., 2009. Geomatrical implication of the CME Earthward direction parameter and its comparison with cone model parameters. *J. Korean Astron. Soc.,* Volume 42, pp. 27-32.

Odstrcil, D., 2003. Modeling 3-D solar wind structure.. *Advances in Space Research,* Volume 32, pp. 497-506.

Plunkett, S. P., Thomson, B. J., St. Cyr, O. C. & Howard, R. A., 2001. Solar source regions of coronal mass ejections and their geomagnetic effects. *J. Atmos. Sol.-Terr. Phys.,* Volume 63, pp. 389-402.

Richardson, I. G. & Cane, H. V., 2010. Near-Earth Interplanetary Coronal Mass Ejections during solar cycle 23 (1996-2009): Catalog and Summary properties. *Solar Phys.,* Volume 264, pp. 189-237.

Robbrecht, E. & Berghmans, D., 2004. Automated recognition of coronal mass ejections (CMEs) in near-real-time data. *A&A,* Volume 425, pp. 1097-1106.

Robbrecht, E., Berghmans, D. & Van der Linden, R. A. M., 2009. Automated LASCO CME catalog for solar cycle 23: are CMEs scale invariant?. *ApJ,* Volume 691, pp. 1222-1234.

Schwenn, R., Dal Lago, A., Huttenen, E. & Gonzalez, W. D., 2005. The association of coronal mass ejections with their effects near the Earth. *Ann. Geophys,* Volume 23, pp. 1033-1059.

Shen, C. et al., 2014. Full-halo coronal mass ejections: arrival at the Earth. *J. Geophys. Res. Space Physics,* Volume 119.

Skirgiello, M., 2005. The east-west asymmetry in coronal mass ejections: evidence for active longitudes. *Ann. Geophys.,* Volume 23, pp. 3139-3147.

Song, H. et al., 2006. The automatic predictability of super geomagnetic storms from halo CMEs associated with large solar flares. *Sol. Phys.,* Volume 238, pp. 141-165.

Srivastava, N. & Venkatakrishnan, P., 2002. Relationship between CME speed and geomagnetic storm intensity. *Geophys. Res. Lett.,* 29(9), p. 1287.

Srivastava, N. & Venkatakrishnan, P., 2004. Solar and interplanetary sources of major geomagnetic storms during 1996-2002. *J. Geophys. Res.,* Volume 109, p. A10103.

St. Cyr, O. C. et al., 2000. Properties of coronal mass ejections: SOHO LASCO observations from January 1996 to June 1998. *J. Geophys. Res.,* 105(A8), pp. 18,169-18,185.

Venkatakrishnan, P. & Ravindra, B., 2003. Relationship between CME velocity and active region magnetic energy. *Geophys. Res. Lett.,* 30(23), p. 2181.

Vrnsak, B. & Zic, T., 2007. Transit times of interplanetary coronal mass ejections and the solar wind speed. *Astron. Astrophys.,* Volume 472, pp. 937-943.

Vrnsak, B. et al., 2012. Propagation of interplanetary coronal mass ejections: The drag-based model. *Solar Phys.,* pp. 1-21.

Wang, Y. et al., 2011. Statistical study of coronal mass ejection source locations: Understanding CMEs viewed in coronagraphs. *J. Geophys. Res.,* Volume 116, p. A04104.

Wang, Y. M. et al., 2002. A statistical study on the geoeffectiveness of Earth-directed coronal mass ejections from March 1997 to December 2000. *J. Geophys. Res.,* 107(A11), p. 1340.

Yashiro, S. et al., 2004. A ctalog of white light coronal mass ejections observed by the SOHO spacecraft. *J. Geophys. Res.,* Volume 109, p. A07105.

Yermolaev, Y. I. & Yermolaev, M. Y., 2006. Statistic study on the geomagnetic storm effectiveness of solar and interplanetary events. *Adv. Space Res.,* Volume 37, pp. 1175-1181.

Zhang, J. et al., 2007. solar and interplanetary sources of major geomagnetic storms (Dst ≤ -100 nT) during 1996-2005. *J. Goephys. Res.,* Volume 112, p. A10102.